Journal of Statistical Mechanics: Theory and Experiment
An IOP and SISSA journal

Quantum phase transition and sliding Luttinger liquid in coupled t–J chains

S Moukouri

Department of Physics and Michigan Center for Theoretical Physics, University of Michigan, 2477 Randall Laboratory, Ann Arbor, MI 48109, USA
E-mail: moukouri@umich.edu

Received 27 October 2005
Accepted 25 April 2006
Published 25 May 2006

Online at stacks.iop.org/JSTAT/2006/P05007
doi:10.1088/1742-5468/2006/05/P05007

Abstract. Using a recently proposed perturbative numerical renormalization-group algorithm, we explore the connection between quantum criticality and the emergence of Luttinger liquid physics in t–J chains coupled by frustrated interactions. This study is built on an earlier finding that at the maximally frustrated point the ground state of weakly coupled Heisenberg chains is disordered, with the transverse exchanges being irrelevant. This result is extended here to transverse couplings up to $J_\perp = 0.6$, and we argue that it may also be valid at the isotropic point. A finite size analysis of coupled Heisenberg chains in the vicinity of the maximally frustrated point confirms that the transverse spin–spin correlations decay exponentially while the longitudinal ones revert to those of decoupled chains. We find that this behaviour persists upon moderate hole doping $x \lesssim 0.25$. For larger doping, the frustration becomes inactive and the quantum critical point is suppressed.

Keywords: density matrix renormalization group calculations, quantum phase transitions (theory)

1742-5468/06/P05007+27$30.00

Contents

1. Introduction

In a number of materials including cuprate high temperature superconductors [1], organic [2] and inorganic [3] quasi-one-dimensional (1D) conductors, the physics is dominated by the combined effect of low dimensionality, strong electron correlations and competing orders. These materials display a phenomenology, in the metallic state above the ordered states, which departs from the Fermi liquid (FL) picture. This has motivated a search for a new paradigm which goes beyond FL theory. Two new ideas, electron fractionalization [4, 5] and quantum criticality (QC) [6], have been proposed as the possible physical effects which may lead to the observed non-FL behaviour.

The breakdown of the FL theory is known to occur in 1D where the low energy physics is described by Luttinger liquid (LL) theory. The LL is fundamentally different from an FL; for instance, instead of the quasiparticle peak displayed by the FL at zero energy in the spectral weight function, a pseudogap is observed in the LL. This is because in the LL the low energy excitations are collective spin density and charge density, in contrast to the FL, where they are still electron-like. An interpretation of this phenomenon is that the electron fragments into density waves known as spinons and holons, which propagate with different velocities. The LL would thus be the natural starting point to search for

J. Stat. Mech. (2006) P05007

non-FL behaviour in higher dimensions. However, it has been impossible to find an LL in dimensions greater than one using perturbative methods. This has been tried by starting from 1D models coupled by a small transverse hopping [7] or directly from the 2D non-interacting electron gas, in which the interaction is introduced perturbatively [8]. It was found in both cases that the FL is the stable fixed point. An alternative strategy applied recently is to build an LL fixed point in anisotropic 2D systems by coupling 1D LLs by marginal transverse strong forward density–density or current–current couplings [9]–[11]. The new 2D fixed point, called the sliding LL (SLL), retains the physics of the 1D LL. It was shown that there is a regime of parameters in which Josephson, charge and spin density waves and single particle hopping are irrelevant, i.e., a domain of stability of the 2D LL. There has not been, to the author's knowledge, any detailed analysis as to why these two approaches lead to conflicting conclusions. It would appear that using simple perturbation theory one cannot go smoothly from a single chain to an SLL.

A different approach has been to assign the departure from an FL behaviour to the proximity of a quantum critical point (QCP) [6]. Because of the proximity of the QCP the adiabatic continuity concept, which is the basis of the FL theory, is no longer valid. In the normal state, the eigenstates of the system are a mixture of states which evolve separately into the ground states existing on the two sides of the QCP. Because of this mixture, the single-particle excitations of the system are not simple electron-like excitations as in the FL.

Considering the pure spin one-half limit of the problem, various studies have found that any small exchange leads to the onset of long-range order. Laughlin [12] has argued that spin-1/2 systems have the propensity to order and it is only at a QCP that they do not. Yet considering that experiments clearly show a departure from the FL, one can still retain the electron fractionalization hypothesis as the driving mechanism of the non-FL but attribute it not to LL physics but to the presence of a QCP. This suggests that in constructing a model Hamiltonian for coupled LLs one must include competing interactions that preclude any order at the QCP.

The difference between the SLL and QCP physics is ultimately two different views of the same reality. If they are both correct, they should emerge from a well controlled study of an appropriate microscopic Hamiltonian. The two-step density-matrix renormalization group (TSDMRG) [13, 14] offers a new approach to study these issues. Although it is a perturbative approach, it has the important non-perturbative property that it can lead to an ordered state starting from a disordered state [14, 15]. Thus it has the ability to treat effectively the different ground states that may arise in weakly coupled chains.

In this paper, we apply the TSDMRG to study the QPT in the spatially anisotropic t–J–$t_\perp$–$J_\perp$–J_d model. We show that in this model the concept of LL can be unified with that of quantum criticality, namely that the model undergoes a QPT at $J_\mathrm{d} = J_\perp/2$ (these couplings are defined in the Hamiltonian (1) given below). At the QCP the system is in a state made of nearly disconnected chains that can be interpreted as an SLL. We first analyse the half-filling case, which corresponds to the anisotropic J_1–J_2 model. We show that the dimerization found in previous approximate field theory analyses [16, 17] does not occur. We then study the doped case at hole densities up to $x = 0.4$. The picture observed in the half-filled case remains valid at moderate dopings. At the QCP, the transverse spin–spin correlation function decays exponentially as in the half-filled case. But at higher dopings, the frustration becomes ineffective and the transition is suppressed;

J. Stat. Mech. (2006) P05007

the ground state is a spin density wave at all couplings. This suggests the existence of an SLL to FL crossover at finite temperature.

2. Model and method

The anisotropic t–J–$t_\perp$–$J_\perp$–J_d model is

$$\begin{aligned} H = &-t\sum_{i,l}(c^\dagger_{i,l}c_{i+1,l} + \mathrm{h.c.}) + J\sum_{i,l}\mathbf{S}_{i,l}\mathbf{S}_{i+1,l} - \tfrac{1}{4}n_{i,l}n_{i+1,l} \\ &- t_\perp\sum_{i,l}(c^\dagger_{i,l}c_{i,l+1} + \mathrm{h.c.}) + J_\perp\sum_{i,l}\mathbf{S}_{i,l}\mathbf{S}_{i,l+1} - \tfrac{1}{4}n_{i,l}n_{i,l+1} \\ &+ J_\mathrm{d}\sum_{i,l}\mathbf{S}_{i,l}\mathbf{S}_{i+1,l+1} + \mathbf{S}_{i+1,l}\mathbf{S}_{i,l+1} \end{aligned} \tag{1}$$

where t and $J > 0$ are the in-chain hopping and exchange parameters; $t_\perp$ and $J_\perp > 0$ are the transverse hopping and exchange parameters; $J_\mathrm{d} > 0$ is the diagonal exchange parameter. We start by describing the extension to fermion systems of the numerical renormalization method, which has been applied so far only to spin systems [13, 14]. There is no significant difficulty in going from spins to fermions. One should simply be careful to consistently apply fermion anticommutation rules. It is crucial to choose an order for the sites in the 2D lattice and keep it throughout the derivation of the algorithm. The method is a special case of a more general matrix perturbation method based on the Kato–Bloch expansion [20, 21], which was recently introduced by the author [15]. The method has two main steps. In the first step, the usual 1D DMRG method [22] is applied to find a set of low lying eigenvalues ϵ_n and eigenfunctions $|\phi_n\rangle$ of a single chain. In the second step, the 2D Hamiltonian is then projected onto the basis constructed from the tensor product of the $|\phi_n\rangle$. This projection yields an effective one-dimensional Hamiltonian for the 2D lattice,

$$\begin{aligned} \tilde{H} \approx &\sum_{[n]} E_{\|[n]}|\Phi_{\|[n]}\rangle\langle\Phi_{\|[n]}| - t_\perp\sum_{i,l}(\tilde{c}^\dagger_{i,l}\tilde{c}_{i,l+1} + \mathrm{h.c.}) \\ &+ J_\perp\sum_{il}\tilde{\mathbf{S}}_{i,l}\tilde{\mathbf{S}}_{i,l+1} - \tfrac{1}{4}\tilde{n}_{i,l}\tilde{n}_{i+1,l} \\ &+ J_d\sum_{il}\tilde{\mathbf{S}}_{i,l}\tilde{\mathbf{S}}_{i+1,l+1} + \tilde{\mathbf{S}}_{i+1,l}\tilde{\mathbf{S}}_{i,l+1}, \end{aligned} \tag{2}$$

where $E_{\|[n]}$ is the sum of eigenvalues of the different chains, $E_{\|[n]} = \sum_l \epsilon_{n_l}$; $|\Phi_{\|[n]}\rangle$ are the corresponding eigenstates, $|\Phi_{\|[n]}\rangle = |\phi_{n_1}\rangle|\phi_{n_2}\rangle\cdots|\phi_{n_L}\rangle$; $\tilde{c}^\dagger_{i,l}$, $\tilde{c}_{i,l}$, and $\tilde{\mathbf{S}}_{i,l}$ are the renormalized matrix elements in the single chain basis. They are given by

$$(\tilde{c}^\dagger_{i,l})^{n_l,m_l} = (-1)^{n_i}\langle\phi_{n_l}|c^\dagger_{i,l}|\phi_{m_l}\rangle, \tag{3}$$

$$(\tilde{c}_{i,l})^{n_l,m_l} = (-1)^{n_i}\langle\phi_{n_l}|c_{i,l}|\phi_{m_l}\rangle, \tag{4}$$

$$\tilde{\mathbf{S}}^{n_l,m_l}_{i,l} = \langle\phi_{n_l}|\mathbf{S}_{i,l}|\phi_{m_l}\rangle, \tag{5}$$

Table 1. Ground-state energies as functions of m and J_d for $J_\perp = 0.2$ and $L = 12$.

m	$J_\mathrm{d} = 0$	$J_\mathrm{d} = 0.114$
32	−0.437 96	−0.428 98
64	−0.439 28	−0.429 17
96	−0.439 70	−0.429 20
∞	−0.440 51	−0.429 21
QMC	−0.440 75	

where n_i represents the total number of fermions from sites 1 to $i-1$. For each chain, operators for all the sites are stored in a single matrix

$$\tilde{c}_l^\dagger = (\tilde{c}_{1,l}^\dagger, \ldots, \tilde{c}_{L,l}^\dagger), \tag{6}$$

$$\tilde{c}_l = (\tilde{c}_{1,l}, \ldots, \tilde{c}_{L,l}), \tag{7}$$

$$\tilde{\mathbf{S}}_l = (\tilde{\mathbf{S}}_{1,l}, \ldots, \tilde{\mathbf{S}}_{L,l}). \tag{8}$$

Since the in-chain degrees of freedom have been integrated out, the interchain couplings are between the block matrix operators in equations (6)–(8) which depend only on the chain index l. In this matrix notation, the effective Hamiltonian is one dimensional and it is also studied by the DMRG method. The only difference from a normal 1D situation is that the local operators are now $m \times m$ matrices, where m is the number of states kept to describe the single chain. In this study, mostly exact diagonalization (ED) instead of DMRG is used in the 1D part of the algorithm. This has the obvious advantage that all the eigenvectors and eigenvalues are known up to a well defined accuracy which is set to 10^{-6} in the Davidson algorithm used to obtain them. The two-step DMRG method is variational [14, 18, 19], so the results can systematically be improved by increasing m. In this study, the calculations were done on a Dell 670 dual Xeon (3.4 GHz) workstation with 4GB of RAM. The maximum m we can reach for the calculations to run within a reasonable time (about three days) is about $m = 96$ for an $L \times (L+1)$ lattice with $L = 16$.

In this study, we are mostly concerned with the parameter regime where $J_\mathrm{d} \approx J_\perp/2$. It is in this regime that the sign problem in the QMC is the most severe. In [18], we have shown that the two-step DMRG is at its best in the highly frustrated regime where QMC simulations cannot be done. To illustrate this fact, we show in table 1 the ground state energy (E_G) as a function of m for the unfrustrated case, with $J_\perp = 0.2$ and $J_\mathrm{d} = 0$, and in the frustrated case at the maximally frustrated point (this point is defined below), with $J_\perp = 0.2$ and $J_\mathrm{d} = 0.114$, for a 12×13 lattice. The extrapolated value of E_G in the unfrustrated case is in good agreement with the QMC. It can be seen that E_G converges faster in the frustrated case. The strategy in this study is to increase $J_\perp$ while the ratio $J_\mathrm{d}/J_\perp$ remains close to 0.5. We do not expect a significant decrease in accuracy for larger $J_\perp$ because, as we will see below, the interchain correlations decay exponentially in this region. Thus despite its perturbative nature, the TSDMRG is able to treat model (1) well beyond the weak coupling regime *as long as one stays in the vicinity of the QCP.*

The high accuracy enjoyed at half-filling is somewhat reduced in the doped case. The reason behind this reduction is simply that the size of the total Hilbert space increases as one goes from two degrees of freedom per site to three. Since we keep roughly the same

J. Stat. Mech. (2006) P05007

Table 2. Hole densities, corresponding exchange couplings and energy differences between charge sectors for $L = 16$.

x	J	$E(N) - E(N+1)$	$E(N) - E(N-1)$
0.125	1.4	0.1012	0.1250
0.25	1.14	0.0982	0.1658
0.375	0.75	0.1355	0.1615

number of states in the two cases, the accuracy will be smaller for doped systems. This can be seen, for instance, when $m = 96$ states are kept in the second step. The energy width of the retained states drops from $\Delta E \approx 1.6$ at half-filling to $\Delta E \approx 0.8$ when the doping is $x = 0.125$ for an $L = 16$ system. Another difficulty which arises upon doping is that one needs to target, during the first step of the algorithm, at least three charge sectors in order to keep matrix elements which involve interchain hopping. A typical situation is $L = 16$ and $x = 0.125$, where the corresponding ground state has 14 electrons. For this charge sector, five spin sectors with $S_Z = 0, \pm 1, \pm 2$ were targeted. For charge sectors with 13 and 15 electrons, four spin sectors with $S_Z = \pm 0.5, \pm 1.5$ were also targeted. Unlike the half-filled case, ED was not done for all doped systems in the first step. For instance, for $L = 16$ we kept 243 states. This number of states corresponds to an exact diagonalization of 12 sites, which means three DMRG iterations were necessary to reach the desired size. Hence, the truncation error at the end of the first step increases from zero at half-filling to about 1×10^{-6} in the doped case.

Removing or adding one electron on a finite system can significantly affect the density if the system size is not large enough. For instance, during the study of an $L = 16$ lattice with the hole density $x = 0.125$, the nominal ground state has 14 electrons, whereas the ground states with 13 and 15 electrons correspond to the hole densities 0.1875 and 0.0625 respectively. Thus, adding or removing holes on small systems induces large variations of the hole density, resulting in large differences between the ground states of the different charge sectors. These variations are the largest near half-filling for small values of J. As a consequence, the electrons cannot jump between the chains and the charge degrees of freedom remain decoupled for small values of the interchain hopping. It is necessary to fine tune J so that these energy differences are smaller than or of the same magnitude as $t_\perp$. For $t_\perp = 0.2$, which will be used for all doped systems, J was chosen so that the difference δ_c between ground state energy of charge sectors differing by one electron is such that $\delta_c \lesssim 0.16$. Fixing δ_c amounts to fixing the chemical potential instead of the coupling. The value of J which satisfies this criterion depends on the hole density x. These values are listed in table 2 for $L = 16$ systems.

3. Finite size analysis at the critical point at half-filling

The half-filled case corresponds to weakly coupled Heisenberg chains that we studied in [14]. In that study it was found that the model displays two phases: a Néel $Q = (\pi, \pi)$ when $J_\mathrm{d}/J_\perp \lesssim 0.5$ and a Néel $Q = (\pi, 0)$ when $J_\mathrm{d}/J_\perp \gtrsim 0.5$. These two phases are separated by a critical point where the long-distance behaviour of the spin–spin correlations along the chains in the 2D system is identical to those in the disconnected

chains. In this study, we will show that this behaviour found for small $J_\perp \lesssim 0.2$ extends well beyond the weak interchain coupling regime (up to $J_\perp = 0.6$). The nature of the ground state in this regime, which was previously called 'nearly independent chains', will be further clarified by the analysis of the interchain spin–spin correlations. Before starting the finite size analysis, it is important to stress the fact that the open boundary conditions (OBCs) which were applied in most of this study create some difficulty in the interpretation of data. While OBCs have the advantage of yielding higher accuracy in DMRG simulations, they artificially break the lattice translational symmetry. The OBCs thus introduce a spurious dimerization d in the 1D chain, as we will see below, which converges very slowly toward zero. To our knowledge, the exact behaviour of this dimerization as a function of the system size has not been reported in the literature. On top of this difficulty, one must account for logarithmic corrections to the finite size quantities. For instance, fitting d with $1/L$, one finds that d extrapolates to a finite value in the limit $L \to \infty$. This deviation from zero, which is the true limit, is the signature of logarithmic corrections. Logarithmic corrections in an open Heisenberg chain have been studied in [28]. They are due to marginally irrelevant operators and their mathematical form is hard to find exactly for small systems. A functional form exists only in the limit of large L. For instance, the finite size spin gap has the following form:

$$\Delta_L \approx \frac{\pi v}{L}\left[1 - \frac{4\pi g(L)}{\sqrt{3}}\right] \tag{9}$$

where $v = \pi/2$ is the spin velocity and $g(L)$ a function such that

$$g(L) \to \frac{\sqrt{3}}{4\pi \log L} \tag{10}$$

when L is very large. For small chains, $g(L)$ has to be introduced as an unknown parameter which is obtained by fitting the data to known limits. Since the main interest of this study lies in the relative behaviour of the 2D system with respect to an isolated 1D chain, we will not use $g(L)$ during the finite size analysis. When performing the finite size analysis, simple linear or quadratic functions of $1/L$ will be used in most cases even though they do not lead to the exact values in the thermodynamic limit for the 1D system because of the logarithmic corrections. We used logarithmic fits when the size of the system was large enough.

3.1. Ground-state energies

The ground-state energies shown in figure 1 show similar behaviour for all values of $J_\perp$ when J_d is varied. Starting from $J_\mathrm{d} = 0$ where the ground state is a Néel $Q = (\pi, \pi)$ phase, E_G typically increases with J_d until it reaches a maximum, labelled the maximally frustrated point $J_\mathrm{d}^{\max}$. Then E_G decreases when $J_\mathrm{d} > J_\mathrm{d}^{\max}$, where the ground state is in a Néel $Q = (\pi, 0)$ phase. The ratio $J_\mathrm{d}^{\max}/J_\perp$ depends on both $J_\perp$ and L. For small $J_\perp$, $J_\mathrm{d}^{\max}/J_\perp$ remains very close to 0.5 but deviates from this value as $J_\perp$ increases. Previous studies (see [23] for a review) found $J_\mathrm{d}^{\max}/J_\perp = 0.6$ when $J_\perp = 1$. This deviation is larger for OBC than for PBC. This is because the maximally frustrated point corresponds to the point where the transverse component of the Fourier transform of the coupling

$$J(Q) = 2\cos Q_x + 2\cos Q_y[J_\perp + 2J_\mathrm{d}\cos Q_x] \tag{11}$$

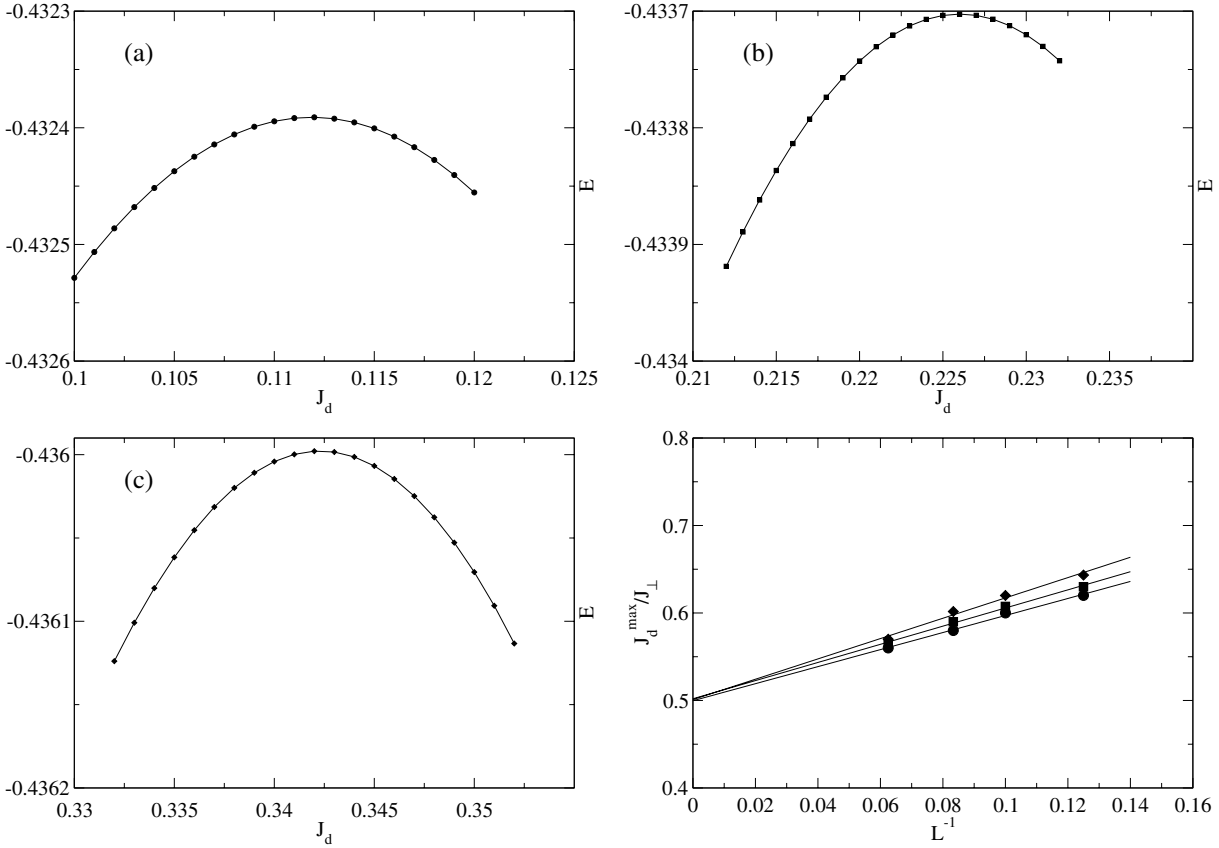

Figure 1. Ground-state energies for $L = 16$ and $J_\perp = 0.2$ (a), $J_\perp = 0.4$ (b) and $J_\perp = 0.6$ (c). Position of the maxima of the ground-state energies as a function of the lattice size for $J_\perp = 0.2$ (circles), $J_\perp = 0.4$ (squares) and $J_\perp = 0.6$ (diamonds) (lower right).

vanishes when $Q_x = \pi$. At this point two J_d bonds cancel one $J_\perp$ bond. But when OBCs are used on a $L \times (L+1)$ lattice, one has L^2 bonds but only $2L(L-1)J_\mathrm{d}$ bonds. Thus for small lattices there is a deficit in J_d bonds which translates into the shift of the maximum towards larger J_d for a fixed $J_\perp$.

This shift has been argued to be indicative of the existence of an intermediate phase, possibly dimerized, in the region between $J_\mathrm{d} = 0.4$ (where the Néel $Q = (\pi, \pi)$ order parameter was found to vanish) and $J_\mathrm{d} = 0.6$ (where the Néel order parameter $Q = (\pi, 0)$ or $(0, \pi)$ vanishes). Our results shown in table 3, which lists the positions of the maxima for various $J_\perp$ and L, indicate that this deviation of $J_\mathrm{d}^{\max}/J_\perp$ from 0.5 is simply a finite size effect. For a fixed L, $J_\mathrm{d}^{\max}/J_\perp$ increases with $J_\perp$ in agreement with the finding in the isotropic case. But one can see that for a fixed $J_\perp J_\mathrm{d}^{\max}/J_\perp$ decreases with L. Figure 1 (lower right) displays the extrapolated values of $J_\mathrm{d}^{\max}/J_\perp$ for $J_\perp = 0.2$, 0.4 and 0.6. They all converge to the vicinity of 0.5. Aside from numerical uncertainties, it is thus likely that $J_\mathrm{d}^{\max}/J_\perp = 0.5$ for all $J_\perp$ in the thermodynamic limit.

The curves of E_G in figure 1 show that E_G is differentiable, which suggests that the transition could be of second order. This is to be contrasted with the pure Ising equivalent of the Hamiltonian (1) obtained by setting all XY terms to zero. E_G for the Ising case

J. Stat. Mech. (2006) P05007

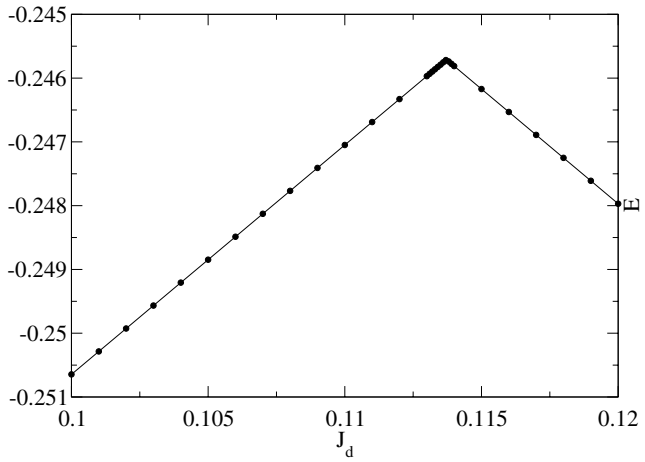

Figure 2. Ground-state energies for $L = 16$ and $J_{z\perp} = 0.2$ in the Ising case.

Table 3. Values of J_d corresponding to the maximum of the ground-state energy for different $J_\perp$ and L.

$J_\perp$	$L = 8$	$L = 10$	$L = 12$	$L = 16$
0.2	0.124	0.119	0.114	0.112
0.4	0.252	0.243	0.236	0.226
0.6	0.386	0.372	0.361	0.342

shown in figure 2 is not differentiable at $J_\mathrm{d}^\mathrm{max}/J_\perp$, as expected since this transition is of first order. It is to be noted that in this case where quantum fluctuations are absent $J_\mathrm{d}^\mathrm{max}/J_\perp$ does not occur at 0.5. This is another fact which favours the conclusion that the deviation from 0.5 seen in previous studies [24] is a finite size effect rather than some subtle quantum effect due to the existence of an intermediate phase between the two Néel ordered states.

3.2. Short-distance spin–spin correlations

The first-neighbour transverse correlation function (figure 3)

$$C_1 = \langle S^z_{il} S^z_{il+1} \rangle \tag{12}$$

taken in the middle of the lattice $(il) = (L/2, L/2+1)$ is linear in the vicinity of $J_\mathrm{d}^\mathrm{max}/J_\perp$ and vanishes at the minimum point J_d^0. Table 4 lists the positions of J_d^0 for various $J_\perp$ and L. These values of J_d^0 are equal to or near $J_\mathrm{d}^\mathrm{max}$ found for E_G for all values of $J_\perp$ studied. We believe that the small differences between the values of J_d^0 and $J_\mathrm{d}^\mathrm{max}$ are due to numerical errors on C_1 and E_G. The differences between these positions are in all cases less than 0.1%. Since the DMRG technique tends to have a better accuracy on the ground-state energies than on the correlation functions, the position of the maximum in E_G is taken as the reference for the transition. The position of the minimum shown in figure 3 (lower right) extrapolates as for E_G towards $J_\mathrm{d}/J_\perp = 0.5$.

At the maximally frustrated point, the spins are such that $C_1 = 0$. This is indeed the best way to minimize frustration. In order to avoid the cost in energy induced by

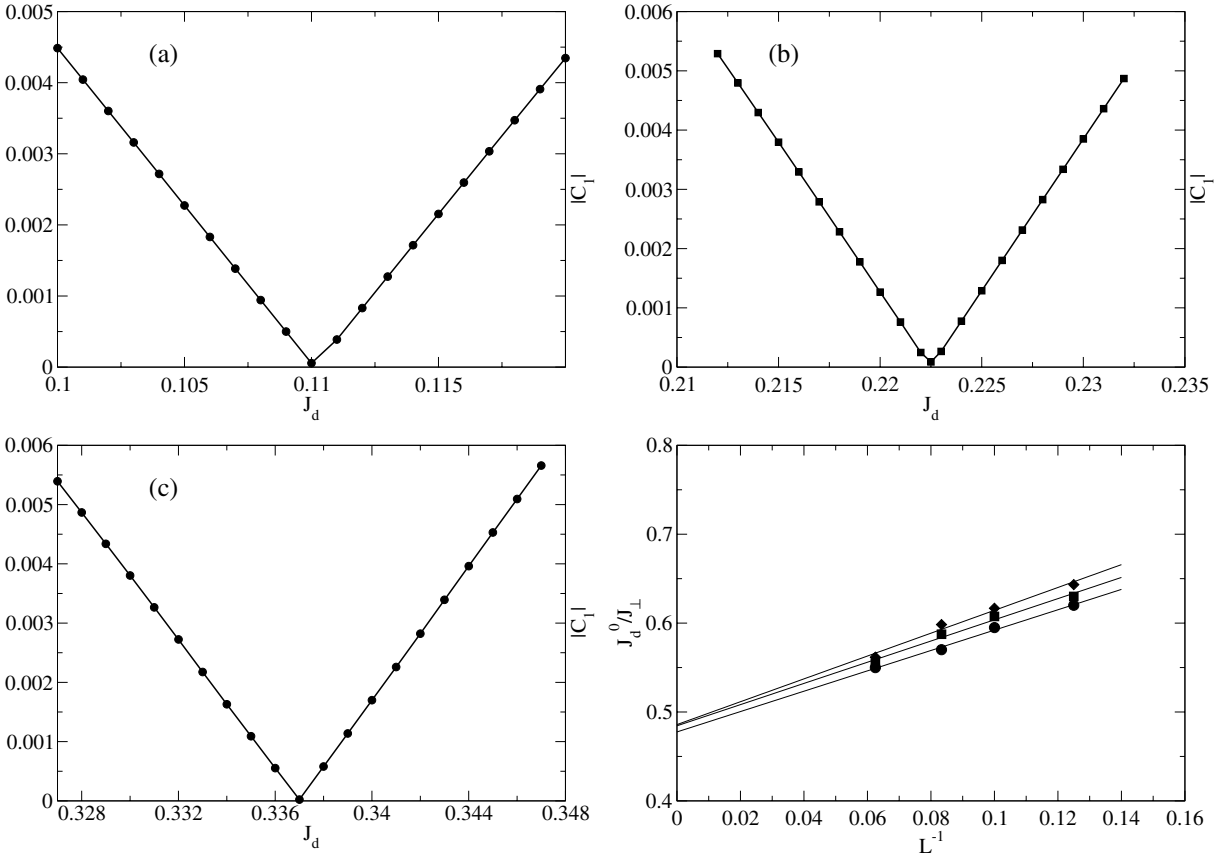

Figure 3. C_1 for $L = 16$ and $J_\perp = 0.2$ (a), $J_\perp = 0.4$ (b) and $J_\perp = 0.6$ (c). Positions of the minima of C_1 as a function of the lattice size for $J_\perp = 0.2$ (circles), $J_\perp = 0.4$ (squares) and $J_\perp = 0.6$ (diamonds) (lower right).

Table 4. Values of J_d corresponding to the minimum of C_1 for different $J_\perp$ and L.

$J_\perp$	$L = 8$	$L = 10$	$L = 12$	$L = 16$
0.2	0.124	0.119	0.114	0.110
0.4	0.252	0.243	0.235	0.222
0.6	0.386	0.372	0.359	0.337

frustrated bonds, the system forms the largest unfrustrated cluster allowable. In this case, the largest unfrustrated clusters are independent chains. This state can actually be seen as the generalization of the Majumdar–Ghosh state known in 1D systems [23]. However, this does not mean that the chains are completely disconnected as in the classical case. In the results on E_G above we were unable to find a point in the parameter space where the ground-state energy of the coupled 2D system is exactly equal to the ground-state energy of disconnected chains. The ground state energies of the 2D systems are always lower than those of completely disconnected chains. This means that despite the fact that $C_1 = 0$, all other transverse correlations are not necessarily zero at $J_\mathrm{d} = J_\mathrm{d}^0$ as in the classical case.

J. Stat. Mech. (2006) P05007

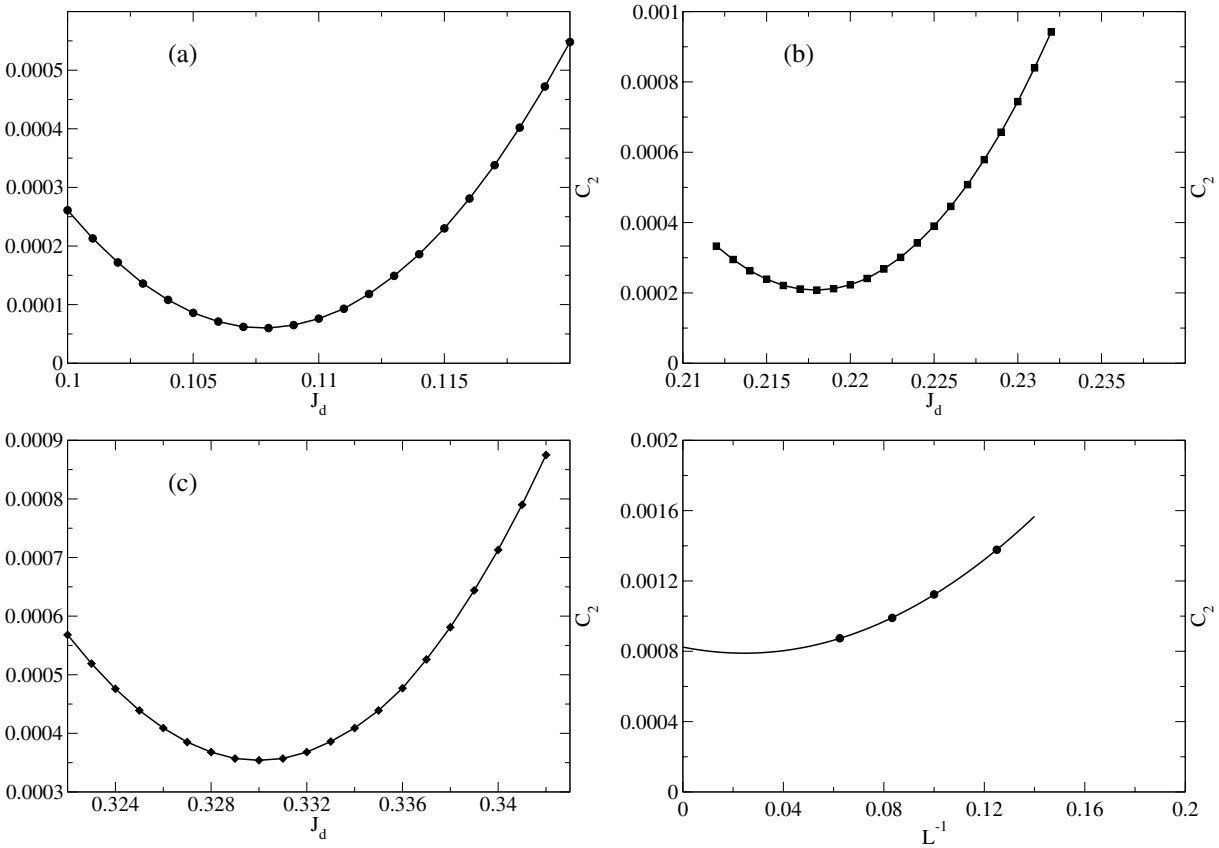

Figure 4. C_2 for $L = 16$ and $J_\perp = 0.2$ (a), $J_\perp = 0.4$ (b) and $J_\perp = 0.6$ (c). Position of the minima of C_2 as a function of the lattice size for $J_\perp = 0.6$ (lower right).

The second-neighbour correlation

$$C_2 = \langle S^z_{il} S^z_{il+2} \rangle \tag{13}$$

shown in figure 4, taken at $(i, l) = (L/2, L/2 + 2)$, does not vanish. It instead has a minimum at $J_{\rm d}^{\rm min}$ for all values of $J_\perp$. The values of C_2 corresponding to $J_{\rm d} = J_{\rm d}^0$ shown in figure 4 (lower right) for $J_\perp = 0.6$ extrapolate to a finite value in the thermodynamic limit. Thus, at the point where $C_1 = 0$, C_2 has a small finite value.

3.3. Dimerization

The examination of the short-range correlations above proves that at the maximally frustrated point there is a weak bond between the chains. The ground state in this region of parameters has been predicted via field theoretic approaches [16, 17] to be a columnar dimer state, with dimerization occurring along the chains. In order to see if dimerization occurs along the chains, we compute the quantity

$$d_{il} = \langle S^z_{2i,l} S^z_{2i+1,l} \rangle - \langle S^z_{2i+1,l} S^z_{2i+2,l} \rangle. \tag{14}$$

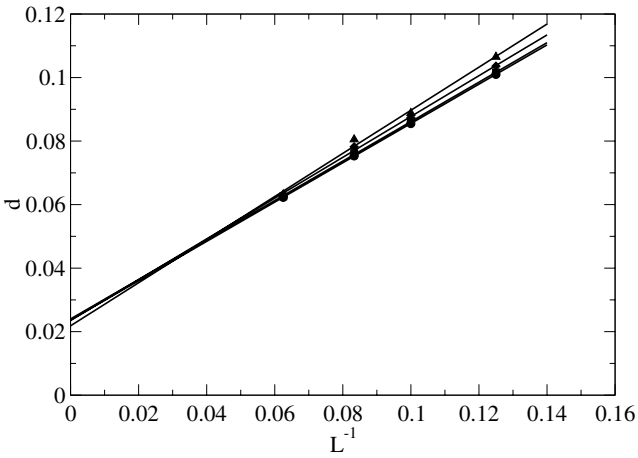

Figure 5. Evolution of the dimerization as function of the lattice size for $J_\perp = 0.$ (circles), $J_\perp = 0.2$ (squares), $J_\perp = 0.4$ (diamonds) and $J_\perp = 0.6$ (triangles).

One should note that since we use OBC, we are in the most favourable situation for dimerization; i.e., the OBC breaks the translational symmetry of the chains and even isolated finite chains are dimerized. This spurious dimerization decays very slowly as $L \to \infty$. It is thus expected that if indeed the system dimerizes at the QCP the finite size behaviour of $d_{i,l}$ of the coupled system will be different from that of isolated chains. In figure 5 d is shown for $J_\perp = 0$, 0.2, 0.4 and 0.6 and for various sizes at $J_{\mathrm{d}}^{\max}$ in the relevant cases. d converges to the same limit whether $J_\perp = 0$ or not. Since the single chain is not dimerized, this shows that the 2D system at the critical point is not dimerized either.

It is important to note that the apparent finite value found for the dimerization in the thermodynamic limit is not due to any limitation of the method used here. This is, as discussed above, the effect of the OBC. The 1D results are exact and results for larger lattices can easily be obtained by using the usual 1D DMRG instead of exact diagonalization. Furthermore, we have shown above how the TSDMRG retains very good accuracy near the maximally frustrated point. The essential physical question is whether the physics of nearly disconnected chains displayed by the 2D systems at the maximally frustrated point for small $J_\perp$ also exists for larger $J_\perp$. Since this physics is governed by short-range competition between different magnetic orientations which lead to virtually zero transverse correlations, one does not really need to go to large systems in order to see the 1D physics. Nevertheless, in order to convince the reader about these conclusions, we have added results on larger lattices (from 12×13 to 64×65) which are shown in figure 6. These results show the influence of logarithmic corrections, signalled by the downturn in d, both for the 1D and 2D systems and are consistent with the fact that d vanishes in the thermodynamic limit in both cases as concluded above. One should note that for larger lattice sizes we did not make a systematic study in order to determine the value of $J_{\mathrm{d}}^{\max}$. $J_{\mathrm{d}}^{\max}$ for a given lattice was obtained using the extrapolation in figure 1 (lower right) from smaller lattices sizes.

We are aware of a different conclusion reached by a recent bosonization approach coupled to a renormalization group and mean-field analyses [17]. In that study for a two-leg ladder in the vicinity of the maximally frustrated point, it was found that although

J. Stat. Mech. (2006) P05007

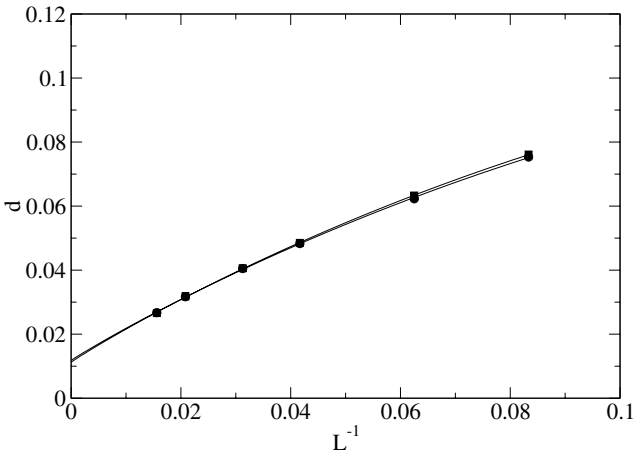

Figure 6. Dimerization for larger lattice sizes for $J_\perp = 0.$ (circles), $J_\perp = 0.2$ (squares) at the maximally frustrated point. The continuous lines are logarithmic fits to the data.

the action of $J_\perp$ is largely cancelled by J_d, at the second order there remain residual couplings $\tilde{J}_1 = 2J_\mathrm{d}^2/\pi^2$ and $\tilde{J}_2 = -3J_\mathrm{d}^2/\pi^2$ which are relevant. $\tilde{J}_1$ favours Néel order and $\tilde{J}_2$, the ring-exchange term, favours a dimerized state. These authors then carried out a self-consistent mean-field approximation of the competition between $\tilde{J}_1$ and $\tilde{J}_2$ in the 2D system. They found a narrow dimerized state between the two ordered magnetic states. According to their conclusions, our prediction of the spin liquid state at the transition is due to finite size effects. But our results above, performed for larger interchain couplings for which the dimerization should be more apparent and is not seen, rather support our conclusions in [14]. There is additional evidence, discussed below, obtained from the study of the three-leg ladder [27], which also agrees with the absence of a dimer phase. It is important to mention that this type of RG analysis is not without a certain bias. The RG transformation usually leads to a proliferation of couplings. There is often some degree of arbitrariness in the choice of the relevant couplings.

3.4. Long-distance spin–spin correlations

Near the maximally frustrated point, the long-distance behaviour of the in-chain spin–spin correlation functions is nearly identical to that of the disconnected chains. These correlations shown in figure 7 for $J_\perp = 0.2$ and $L = 16$ are nearly independent of m. This is because, for a purely 1D system of this size, they are already known with very good accuracy. Since the chains are nearly disconnected, no significant increase of m is required to describe them with the same level of accuracy as in 1D.

This conclusion is supported by the behaviour of the transverse correlation functions shown in figure 8 for the same set of parameters. $C_\perp(i)$ is found to be equal to zero for $i \gtrsim 4$ for all the values of m.

$C_\parallel(i)$ and $C_\perp(i)$ are independent of $J_\perp$ at the maximally frustrated point; i.e., only the ratio $J_\mathrm{d}/J_\perp$ is important up to intermediate values. This is seen in figures 9 and 10, where these quantities are compared for $J_\perp = 0.2$, 0.4 and 0.6. $C_\parallel(i)$ is nearly identical to that of independent chains while $C_\perp(i)$ remains very small and decays exponentially

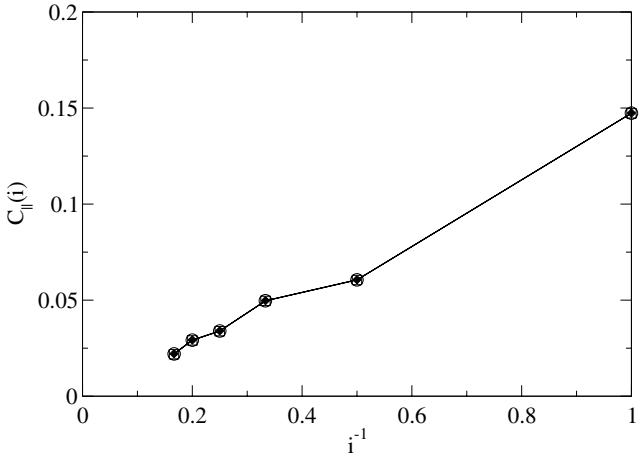

Figure 7. Longitudinal spin–spin correlation at $J_{\mathrm{d}}^{\max}$ as a function of the distance for $L = 16$ and $m = 32$ (circles), $m = 64$ (squares) and $m = 96$ (diamonds).

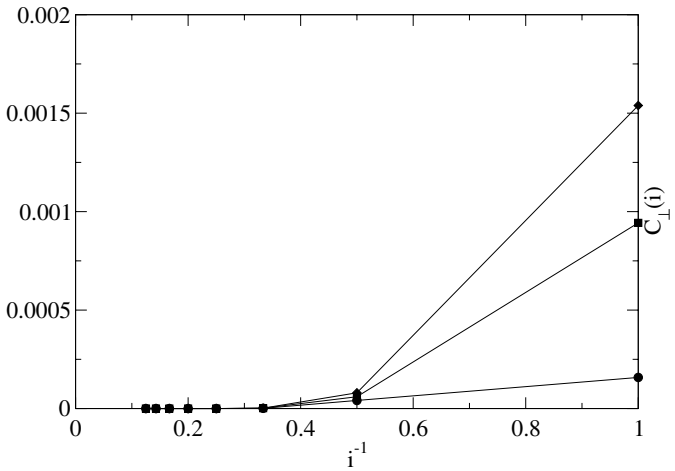

Figure 8. Transverse spin–spin correlation at $J_{\mathrm{d}}^{\max}$ as a function of the distance for $L = 16$ and $m = 32$ (circles), $m = 64$ (squares) and $m = 96$ (diamonds).

with i. This behaviour is valid from weak to intermediate coupling regimes. It is to be noted that since the maximally frustrated point is chosen at the maximum $J_{\mathrm{d}}^{\max}$ of E_{G}, C_1 is not equal to zero because the two quantities differ slightly as shown in tables 3 and 4 because of numerical uncertainties.

It is possible to question our choice of $C_{\perp}(i)$ for the study of the disappearance of the magnetic order. The usual quantity is rather the correlation function along the diagonal direction $C_{\mathrm{d}}(i)$. In figure 11 we show that near the maximally frustrated point $C_{\mathrm{d}}(i)$ displays the same exponential decay as $C_{\perp}(i)$.

This behaviour of $C_{\perp}(i)$ at $J_{\mathrm{d}} \approx J_{\perp}/2$ is to be contrasted to that of the magnetic regime. In figure 12 we see that, for instance, $C_{\perp}(4)$ of the magnetic case is already four orders of magnitude larger than in the disordered case. The exponential decay of $C_{\perp}(i)$ seen in figure 12 and the decay of $C_{\parallel}(i)$, which is nearly that of decoupled chains,

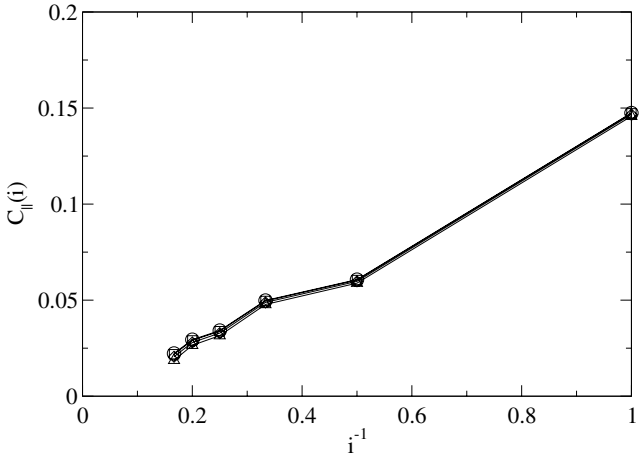

Figure 9. Longitudinal spin–spin correlation at $J_{\mathrm{d}}^{\max}$ as a function of the distance for $L = 16$ for $J_{\perp} = 0.$ (circles), $J_{\perp} = 0.2$ (squares), $J_{\perp} = 0.4$ (diamonds) and $J_{\perp} = 0.6$ (triangles).

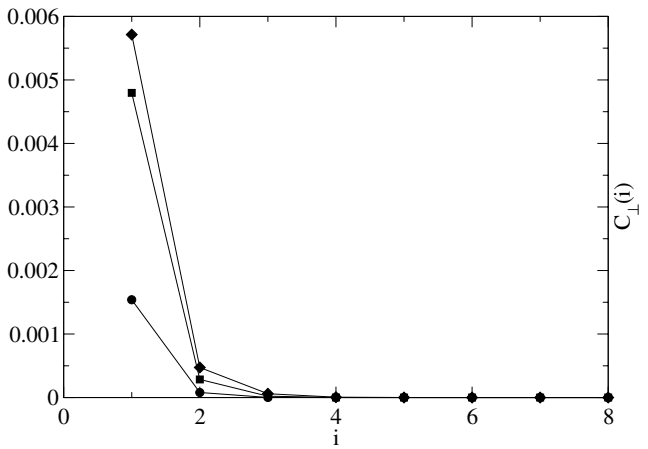

Figure 10. Transverse spin–spin correlation at $J_{\mathrm{d}}^{\max}$ as a function of the distance for $L = 16$ for $J_{\perp} = 0.2$ (circles), $J_{\perp} = 0.4$ (squares) and $J_{\perp} = 0.6$ (diamonds).

suggest that for $J_{\mathrm{d}} \approx J_{\perp}/2$ the system displays a spin analogue of the sliding Luttinger liquid (SLL) discussed in fermionic models [9]–[11]. In the region $J_{\mathrm{d}} \approx J_{\perp}/2$ the two competing magnetic fluctuations (π, π) and $(\pi, 0)$ cancel each other, leading to irrelevant interchain couplings. These irrelevant couplings renormalize the energy but do not modify the behaviour of the correlation functions. Our finding shows that the SLL concept is linked to quantum criticality. It also provides numerical evidence of fractionalization at the critical point as first suggested in [12].

3.5. Finite size spin gap

Logarithmic corrections and the spurious dimerization introduced by the OBC are accompanied by a spurious gap in the pure 1D system. In figure 13 we see that at the maximally frustrated point the gap for $J_{\perp} = 0.2$ converges to the same value as that

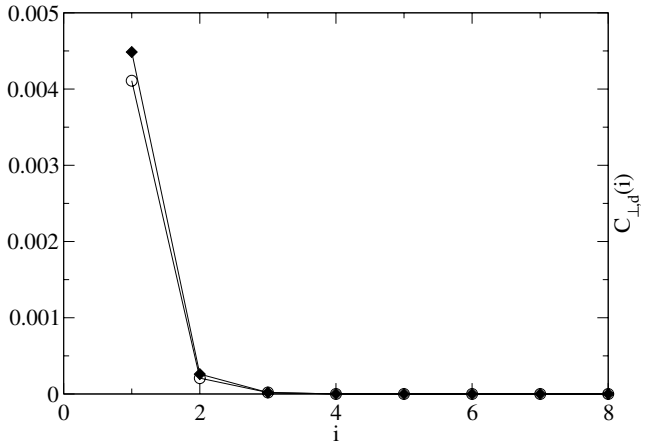

Figure 11. Transverse (diamonds) and diagonal (circles) spin–spin correlation at $J_\perp = 0.2$ and $J_\mathrm{d} = 0.1$ for $L = 16$ as a function of the distance.

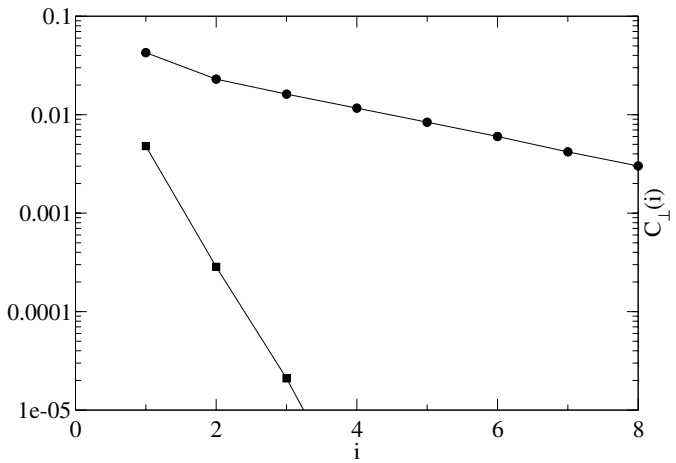

Figure 12. Transverse spin–spin correlation as a function of the distance for $L = 16$ for $J_\perp = 0.4$, $J_\mathrm{d} = 0$ (circles), $J_\perp = 0.4$ and $J_\mathrm{d} = 0.219$ (squares). Note that this value of J_d is not exactly at $J_\mathrm{d}^{\max}$.

of $J_\perp = 0$. It is thus reasonable, knowing that the single chain is gapless, to conclude that the 2D system is also gapless in the thermodynamic limit. We note that the logarithmic corrections are not taken into account in the gaps predicted by exact diagonalization studies [24].

As for the results on dimerization, one might conclude that our method leads to a finite gap in the thermodynamic limit. Again we emphasize that this is not a limitation of the TSDMRG but the consequence of applying the OBC as discussed in the introduction of this section. The study of larger systems up to 64×65, shown in figure 14, again is consistent with the fact that the gap vanishes in the thermodynamic limit at the maximally frustrated point of the 2D system as for the single chain. This illustrates the danger of using relatively small systems as in exact diagonalization studies for the extrapolation to the thermodynamic limit.

J. Stat. Mech. (2006) P05007

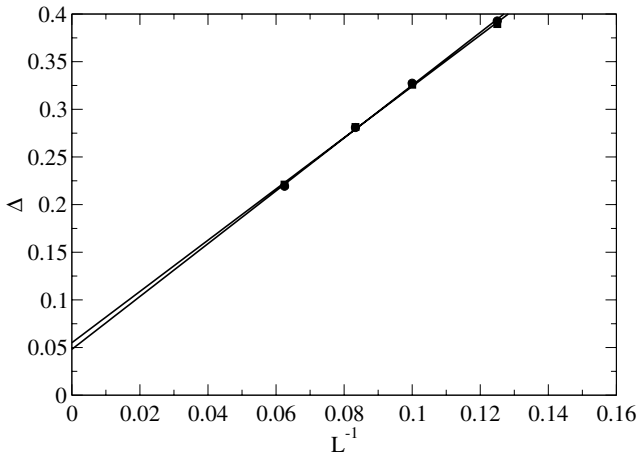

Figure 13. Finite size gap with OBC as a function of the lattice size for $J_\perp = 0$ (circles) and, $J_\perp = 0.2$ (squares) at $J_{\rm d}^{\rm max}$.

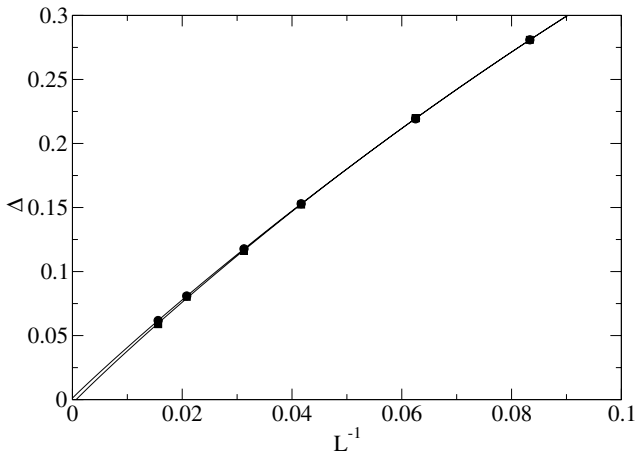

Figure 14. Finite size gap for larger lattices with OBC as a function of the lattice size for $J_\perp = 0$ (circles) and $J_\perp = 0.2$ (squares). The continuous lines are logarithmic fits $a_0 + a_1/L + a_2/(L \log L)$ to the data.

A legitimate criticism of our conclusion could be that the prediction of a gapless state in the thermodynamic limit is an artifact of the TSDMRG. It is well possible that since the single chain is gapless it would not be a good starting point for gapped systems. This would explain our disagreement with [17]. In order to show that the TSDMRG can predict a gap when it exists in the thermodynamic limit, we studied the gap behaviour in the well known case of the two-leg ladder [30]. The results are shown in figure 15 for $J_\perp = 0.2$ and $J_{\rm d} = 0$. It can be seen that in contrast to the 2D situation at the maximally frustrated point the gap for the two-leg ladder has a distinct finite size behaviour. Its curvature as a function of L is positive and the gap extrapolates to a finite value in the thermodynamic limit as expected.

doi:10.1088/1742-5468/2006/05/P05007

J. Stat. Mech. (2006) P05007

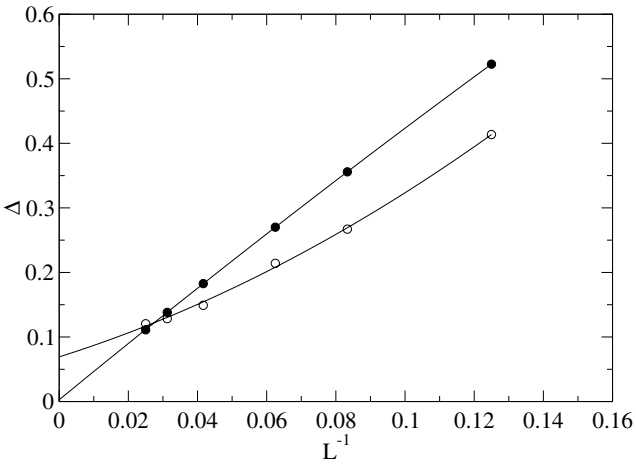

Figure 15. Finite size gap for the two-leg ladder with PBC as a function of L for $J_\perp = 0$ (filled circles) and $J_\perp = 0.2$ (open circles).

3.6. Implications for the isotropic J_1–J_2 model

For the isotropic case ($J_\perp = J$) it is usually said that there is a large amount of evidence supporting the fact that the magnetic order vanishes for $0.4 \lesssim J_\mathrm{d} \lesssim 0.6$, i.e. a spin gapped state exists in this region [23]. But in our opinion, this conclusion is not that compelling. The results displayed above indicate that the limit $J_\mathrm{d}/J_\perp \to 0.5$ is in fact analogous to the problem of coupled unfrustrated chains ($J_\mathrm{d} = 0$ in Hamiltonian (1)) in the limit $J_\perp \to 0$. For this latter problem there was a prediction of a spin liquid state for $J_\perp \lesssim 0.1$ from ED, field theory mapping and spin wave approaches [25]. However, a QMC study [26] later showed that the Néel order extends down to $J_\perp = 0.01$. It is now believed that long-range order sets in as soon as $J_\perp \neq 0$. This suggests that the disordered phase often claimed to exist for the isotropic J_1–J_2 model, which was obtained from ED of up to 6×6 systems or series expansions, is not a settled issue.

In fact there is strong evidence, unfortunately neglected, which points to the contrary. A DMRG study [27] performed on a three-leg ladder found that the system is gapless for all values of $J_\perp$ and J_d. The lengths of the chains were up to $L = 360$ so that finite size effects were negligible. The computed phase diagram has two states: a symmetric doublet phase and a quartet phase. These two states will naturally evolve towards the Néel $Q = (\pi, \pi)$ and $Q = (\pi, 0)$, respectively, when the number of chains goes to infinity. This is fully consistent with our conclusions.

The perturbative method applied in this study cannot be used directly to study the isotropic case, since starting with the decoupled chains is too biased. But if the principles uncovered in the anisotropic case are to be applied, it appears that even in the isotropic situation the nearly decoupled chains ground state is still the best way to minimize frustration. From this consideration, we applied the method to the isotropic case and arrived at the same conclusions as above: namely, that the ground state at the maximally frustrated point is made of nearly disconnected chains and is thus an SLL.

In table 5, we show the ground state energy for $L = 6$ and 8 for different values of m. We applied periodic boundary conditions along the chains and OBC in the transverse

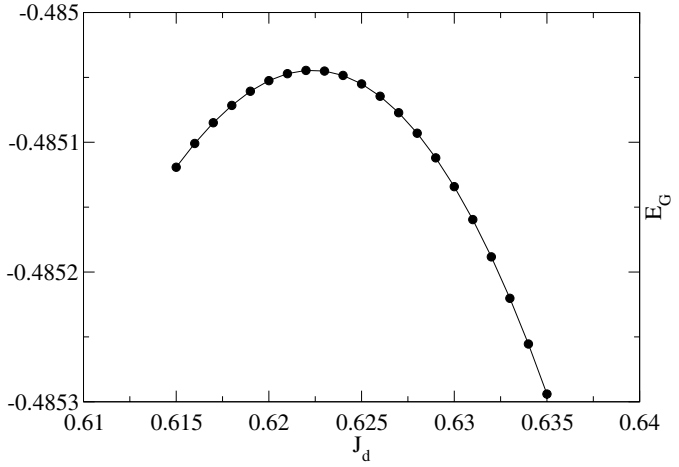

Figure 16. Ground-state energies for $L = 8$ and $J_\perp = 1$ as a function of J_d.

Table 5. E_G for $J_\perp = 1$ and $J_\mathrm{d} = 0$ as a function of m for $L = 6$ and 8 systems.

m	$L = 6$	$L = 8$
16	−0.5910	−0.5647
32	−0.6055	−0.6018
64	−0.6171	−0.6205
80		−0.6261
∞	−0.6322	−0.6420

direction. The final value for E_G at a given size is obtained by extrapolating m to ∞. The results for $L = 4$, 6 and 8 are then extrapolated to yield the TSDMRG estimate of E_G, which is −0.6625. This value is to be compared to the QMC result −0.6699. We have lost two orders of magnitude in accuracy between the TSDMRG and QMC compared to the anisotropic case. For this reason we did not study longer chains since the accuracy decreases when the system size increases for a fixed number of states. However, near the maximally frustrated point, since the physics is again that of nearly disconnected chains as seen below, we can assume that we gain roughly an order of magnitude as for the anisotropic case. This shows that the TSDMRG can reliably describe the transition region for small ($L \lesssim 8$) isotropic systems.

E_G (shown in figure 16), C_1 (figure 17) and $C_\perp(i)$ (figure 18) display the same features as in the anisotropic case. E_G shows a maximum, C_1 vanishes as J_d is increased from zero and C_1 goes from −0.0897 at $J_\mathrm{d} = 0$ to −0.000 06 at $J_\mathrm{d} = 0.634$. But we now find that the positions of $J_\mathrm{d}^\mathrm{max} \approx 0.622$ and $J_\mathrm{d}^0 \approx 0.634$ are somewhat far apart. This probably reflects the fact that our results are less accurate in the isotropic case. For this reason we did not perform the finite size analysis in order to see whether $J_\mathrm{d}^\mathrm{max}$ and J_d^0 both extrapolate to 0.5 as in the anisotropic case. $C_\perp(i)$ in the isotropic limit is shown in figure 18 for $L = 8$. We find that at the maximally frustrated point, this quantity decays exponentially as for smaller value of $J_\perp$.

Another indication for this is the finding by a recent ED study [24] that even at $J_\perp = 0.8J$ the behaviour observed at lower coupling still persists. However, this study

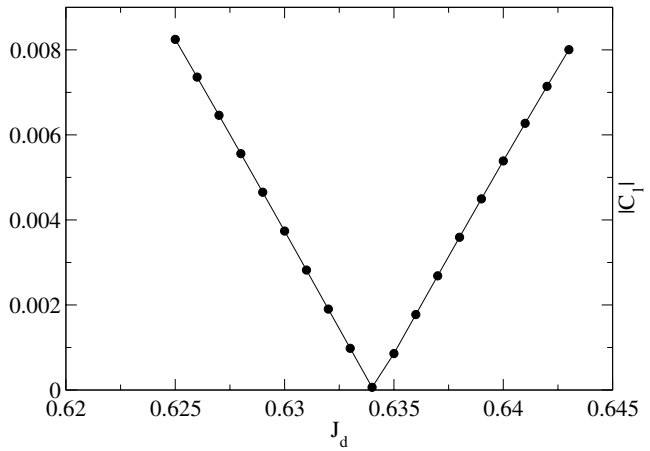

Figure 17. C_1 for $L = 8$ and $J_\perp = 1$ as a function of J_d.

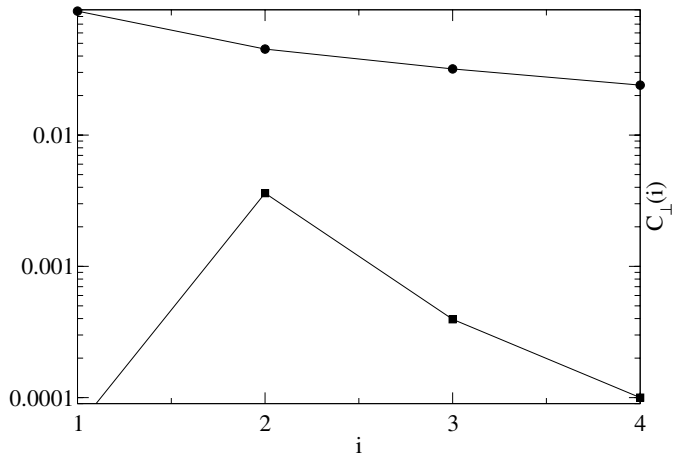

Figure 18. Transverse spin–spin correlation as a function of the distance for $J_\perp = 1$, $J_\mathrm{d} = 0$ (circles), $J_\perp = 1$, $J_\mathrm{d} = 0.634$ (squares) for $L = 8$.

also predicts a spin gap. We believe this apparent contradiction is due to the fact that the ED study was done with an even number of chains and the logarithmic corrections were not considered. The study of the finite size behaviour of the gap near the maximally frustrated point showed that it is crucial to study larger systems in order to get the correct extrapolation to the thermodynamic limit.

4. Doped systems

Having identified the ground state at half-filling as a spin version of an SLL, we now turn to the doped case. We will mostly restrict ourselves to the vicinity of the maximally frustrated point $J_\mathrm{d} \approx J_\perp/2$. This is primarily because the results at half-filling indicate that far from this point no significantly new physics is likely to occur. One would expect that the two Néel ground states found at half-filling away from the QCP will naturally evolve into spin density wave (SDW) ground states upon doping. The really physically interesting question is what the effect of doping is on the spin SLL.

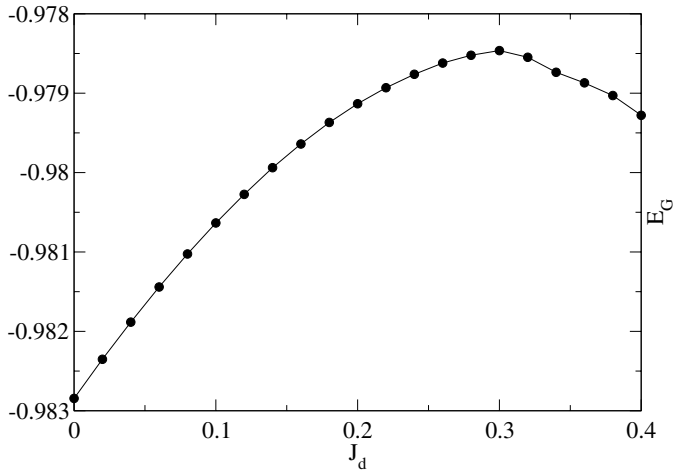

Figure 19. Ground-state energy for $x = 0.167$, $L = 12$ and $J_\perp = 0.4$ as a function of J_d.

The main finding in the doped case is that the magnetic properties of the system do not significantly change as long as one remains close to half-filling. But if the hole doping becomes too large, $x \approx 0.3$, the model displays a qualitative change. The frustration ceases, and J_d cooperates instead of competing with $J_\perp$.

4.1. Ground-state energies

E_G at $x = 0.167$ for $L = 12$ as a function of J_d is shown in figure 19. It displays a maximum as for the half-filled case. One can note that this maximum is now shifted towards higher values of J_d. This maximum goes from $J_\mathrm{d}^{\max} = 0.236$ for $x = 0$ to $J_\mathrm{d}^{\max} = 0.30$ for $x = 0.167$. By inserting the holes, the system becomes less frustrated. It is therefore necessary to increase J_d in order to balance the action of $J_\perp$. We find that if the hole density is increased above $x \approx 0.3$ the maximum in E_G is suppressed. For $x \gtrsim 0.3$, E_G always decreases with J_d. This is seen for instance in figure 20, where E_G for $x = 0.4$ is shown. This shows that for large dopings, in contrast to the near-half-filling situation, J_d increases instead of reducing the stability of the system.

4.2. Short-distance spin–spin correlations

This difference between the near-half-filling and larger hole densities is also displayed in C_1. In figure 21 corresponding to $x = 0.167$, C_1 goes to zero at $J_\mathrm{d}^0 = 0.3$. One may note that there seems to be a jump at the transition point. This jump was not observed at half-filling. This could indicate a possible first-order transition. However this is not supported by the behaviour of E_G shown above. We notice during the simulations that, if one is too close to the transition point, for the same set of parameters, one can go from one side of the transition when the number of chains is small to the other side when the number of chains gets larger. We thus believe that the jump observed in C_1 is somehow related to the reduced accuracy in the doped case induced by the mixture of the two competing ground states near the transition point. The regularity of the curve far from

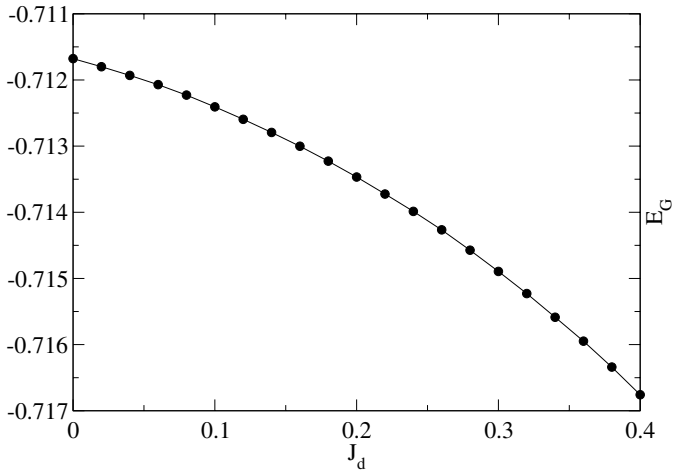

Figure 20. Ground-state energy for $x = 0.4$, $L = 10$ and $J_\perp = 0.2$ as a function of J_d.

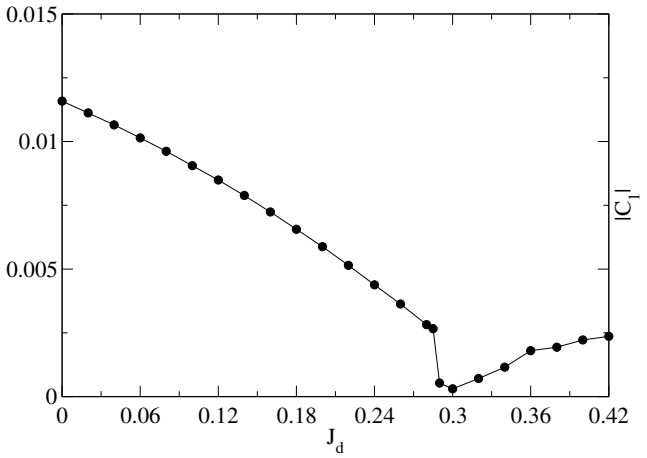

Figure 21. C_1 for $x = 0.167$, $L = 12$ and $J_\perp = 0.4$ as a function of J_d.

the transition point justifies this assumption. In agreement with the behaviour of E_G, the transition is suppressed when the hole doping is too large. C_1 shown in figure 22 always remains antiferromagnetic and increases with J_d.

4.3. Long-distance correlations

$C_\perp(i)$ shown in figure 23 for $x = 0.125$ retains essentially the same behaviour as in the half-filled case. It decays exponentially at the maximally frustrated point for $J_\perp = 0.2$, 0.4 and 0.6 while the decay is significantly slower in the unfrustrated case. In the absence of frustration, $C_\perp(i)$ has an antiferromagnetic signature while $C_\parallel(i)$ is SDW-like with $k_F = (\pi/2)(1 - x)$, where x is the density of holes. Though we have not made a finite size analysis, it is reasonable to believe that the system is in an SDW ground state in the thermodynamic limit. At the maximally frustrated point, the magnetic order parameter vanishes.

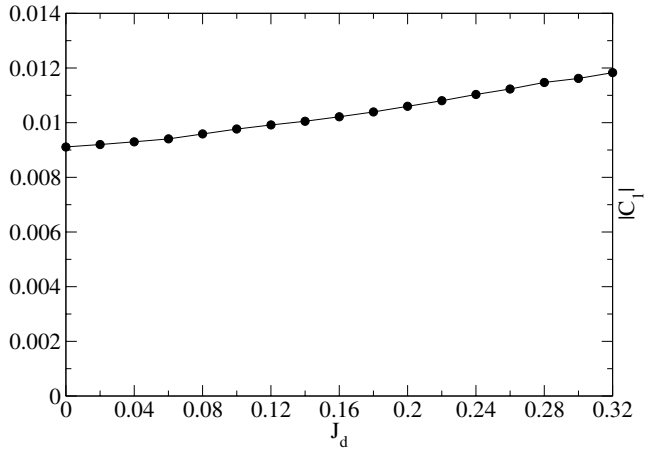

Figure 22. C_1 for $x = 0.4$, $L = 10$ and $J_\perp = 0.2$ as a function of J_d.

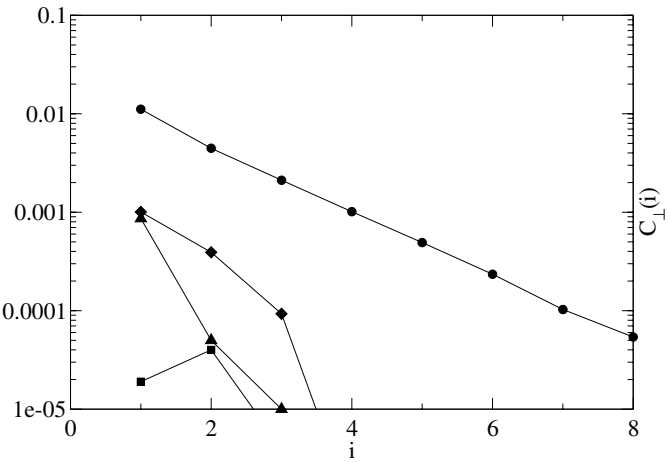

Figure 23. Transverse spin–spin correlation as a function of the distance for $J_\perp = 0.2$, $J_\mathrm{d} = 0$ (circles), and at the maximally frustrated point at $J_\perp = 0.2$ (squares), $J_\perp = 0.4$ (triangles) and $J_\perp = 0.6$ (diamonds) for $x = 0.125$ and $L = 16$.

As x is further increased to 0.167, 0.25 and 0.375, we find that the role of frustration is reduced. Ultimately, the system evolves towards a conventional SDW ground state. This is seen in figure 24, where the exponential decay of $C_\perp(i)$ is significantly slowed at large hole dopings. There is already four orders of magnitude between $C_\perp(4)$ for $x = 0.125$ and 0.375. It appears that the system tends to choose hole configurations that minimize frustration in order to avoid the cost in energy induced by frustration. It is in the vicinity of $x = 0.125$ that frustration is most effective; i.e., the magnetic order which exists in the non-frustrated case can easily be cancelled by frustration. Beyond this point, frustration becomes less and less effective. At quarter filling the system can choose a hole configuration so that frustration becomes ineffective. Since the introduction of holes usually tends to reduce the order parameter, the re-emergence of magnetism at the maximally frustrated point by introduction of holes can be viewed as the manifestation of Villain's order from disorder effect [29].

doi:10.1088/1742-5468/2006/05/P05007

J. Stat. Mech. (2006) P05007

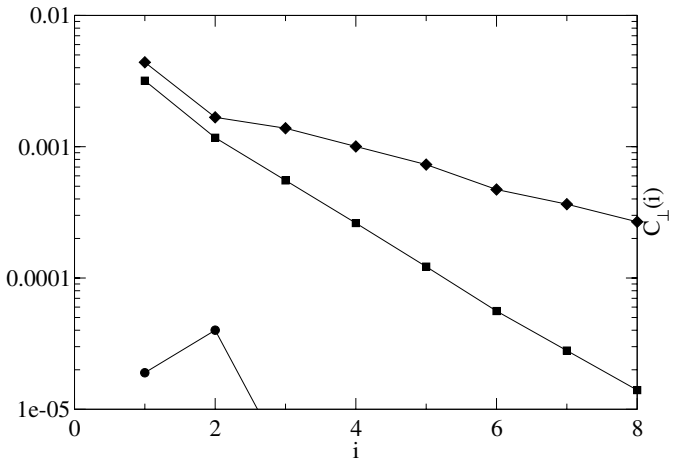

Figure 24. Transverse spin–spin correlation as a function of the distance for $J_\perp = 0.2$, $J_\mathrm{d} = 0.11$ for $x = 0.125$ (circles), $x = 0.25$ (squares) and $x = 0.375$ for $L = 16$.

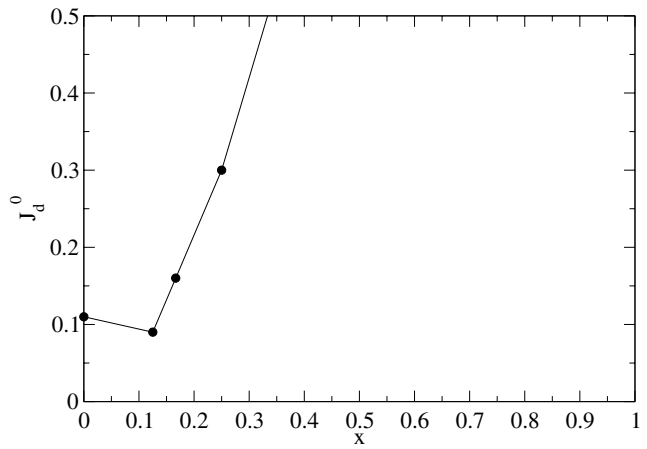

Figure 25. Critical values of J_d as a function of doping.

These arguments are illustrated in figure 25, where the value of J_d^0 is shown as a function of x. $J_\mathrm{d}^0(x)$ first slowly decreases from half-filling until about $x = 0.125$ and then sharply rises. Thus there is a point, for x between 0.25 and 0.5, where the critical point is suppressed.

4.4. Equal-time Green's function

The transition point is also signalled in the equal-time transverse Green's function

$$G_\perp(i) = \langle c_{j,l\sigma} c^\dagger_{j,l+i\sigma} \rangle. \tag{15}$$

$G_1 = G_\perp(1)$ shown in figure 26 decays from $J_\mathrm{d} = 0$ to $J_\mathrm{d} = J_\mathrm{d}^{\max}$. This decay of G_1 is consistent with the tendency to localize the particles within the chains induced by J_d.

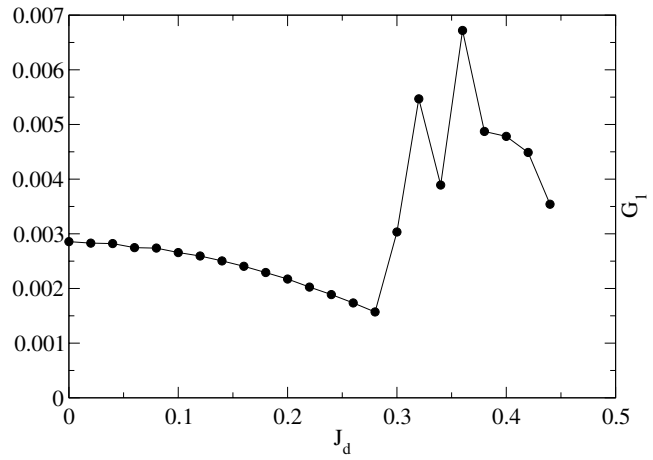

Figure 26. Transverse equal-time first-neighbour Green's function at $x = 0.167$ as a function of J_d for $L = 12$.

However, in the vicinity of $J_\mathrm{d}^{\max}$, the situation becomes less clear. G_1 strongly oscillates. These oscillations cease when J_d is beyond the critical region where G_1 decays again. It appears that G_1 behaves differently in the two ordered states; it increases from the transition point in the first and decreases from the transition point in the second state. The curious behaviour seen in the transition region could well be the manifestation of the mixture of the two ground states seen in E_G and in C_1. This mixture affects the value of fermion correlation functions more severely than their spin counterpart. For this reason, we have not calculated charge density or superconducting correlations which involve four fermions. There is however no reason to suspect a charge density or superconducting ordering in the vicinity of $J_\mathrm{d}^{\max}$. These transitions would be of first order and would thus be apparent in the ground-state energy.

Despite the uncertainties caused by the mixture of the two ground states on the two sides of the transition, we nevertheless show in figure 27 the equal-time transverse Green's function in the SDW case and in the magnetically disordered case. The decay in the disordered state is slower than in the magnetic case. This raises the possibility of the relevance of the single-particle hopping. If true, this would mean that the spin and the charge behave differently in the transverse direction at the transition point. More work needs to be done in order to clarify this point.

5. Conclusions

In this study, we have presented numerical evidence for the connection between the quantum phase transition and Luttinger liquid physics from the study of coupled t–J chains. The ordered $Q = ((1-x)\pi, \pi)$ Néel state that exists at half-filling and near half-filling for $J_\perp \neq 0$ and $J_\mathrm{d} = 0$ is destroyed at $J_\mathrm{d} = J_\mathrm{d}^{\max}$. At this point, the in-chain spin–spin correlation of the 2D system decays nearly like those of independent chains. A careful examination of the transverse spin–spin correlations reveals that the chains are loosely bound and that these correlations decay exponentially. We thus identify the state of the system at this maximally frustrated point as a sliding Luttinger liquid. These properties are observed even when the interchain couplings are well beyond the perturbative regime.

doi:10.1088/1742-5468/2006/05/P05007

J. Stat. Mech. (2006) P05007

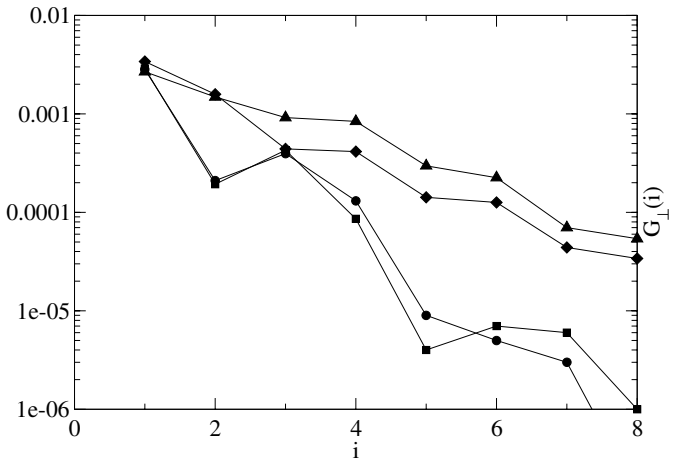

Figure 27. Transverse equal-time Green's function at $x = 0.125$ for $J_\mathrm{d} = 0.2$, $J_\mathrm{d} = 0$ for spins up (circles), spins down (squares); $J_\perp = 0.2$, $J_\mathrm{d} = 0.11$ for spins up (triangles), spins down (diamonds).

The key mechanism behind this connection is magnetic frustration. The leading effect which brings a compromise between the frustrated bonds is the severing of these bonds to form the largest unfrustrated clusters with the lowest energy. These unfrustrated units are then coupled by some residual interactions generated by quantum fluctuations. These residual interactions may or may not drive the system away from the physics displayed by the largest unfrustrated clusters. This picture is in contrast to the widely accepted hypothesis which suggests that the leading mechanism to avoid frustration is short- or long-range dimerization which may (spin–Peierls) or may not (resonating valence bond) lead to the breaking of the lattice translational symmetry. It is however to be noted that the two pictures do not necessarily always conflict with each other. In some models, the largest unfrustrated clusters could just be dimers or plaquettes. Our point here is that this is not the case in the anisotropic J_1–J_2 model.

In the model studied in this paper, LL physics arises at the QCP because the severing of frustrated bonds leads to nearly independent chains which are the largest unfrustrated clusters. These chains are coupled, even when the original interchain couplings are large, only by residual interactions which do not appear to destabilize the 1D physics at the QCP. In a numerical simulation, however, it is impossible to rule out completely the emergence of relevant interchain interactions at a very low energies.

Acknowledgments

We wish to thank M E Fisher, C L Kane, S Kivelson, R B Laughlin and A-M S Tremblay for helpful discussions. We thank S Haas for sharing his t–J ladder data. We also thank J Allen for numerous exchanges during the course of this work. We are grateful to P L McRobbie for reading the manuscipt.

References

[1] Orenstein J and Millis A J, 2000 *Science* **288** 468
[2] Bourbonnais C and Jérome D, 1999 *Advance in Synthetic Metals* ed P Bernier, S Lefrant and G Bidan (New York: Elsevier) p 206

[3] Allen J W, 2002 *Solid State Commun.* **123** 469
[4] Anderson P W, 2000 *Science* **288** 480
[5] Kivelson S, 2002 *Synth. Met.* **125** 99
[6] Sachdev S, 1999 *Quantum Phase Transitions* (Cambridge: Cambridge University Press)
[7] Bourbonnais C and Caron L G, 1991 *Int. J. Mod. Phys.* B **5** 1033
[8] Shankar R, 1994 *Rev. Mod. Phys.* **66** 129
[9] Vishwanath A and Carpentier D, 2001 *Phys. Rev. Lett.* **86** 676
[10] Emery V J, Fradkin E, Kivelson S A and Lubensky T C, 2000 *Phys. Rev. Lett.* **85** 2160
[11] Mukhopadhyay R, Kane C L and Lubensky T C, 2001 *Phys. Rev.* B **64** 045120
[12] Laughlin R B, 1998 *Adv. Phys.* **47** 943
[13] Moukouri S and Caron L G, 2003 *Phys. Rev.* B **67** 092405
[14] Moukouri S, 2004 *Phys. Rev.* B **70** 014403
[15] Moukouri S, 2004 *Phys. Lett.* A **325** 177
[16] Nersesyan A A and Tsvelik A M, 2003 *Phys. Rev.* B **67** 024422
Tsvelik A M, 2004 *Phys. Rev.* B **70** 134412
[17] Starykh O A and Balents L, 2004 *Phys. Rev. Lett.* **93** 127202
[18] Alvarez J V and Moukouri S, 2005 *Int. J. Mod. Phys.* C **16** 843
[19] Moukouri S and Alvarez J V, 2005 *Phys. Lett.* A **344** 387
[20] Kato T, 1949 *Prog. Theor. Phys.* **4** 514
Kato T, 1950 *Prog. Theor. Phys.* **5** 95
[21] Bloch C, 1958 *Nucl. Phys.* **6** 329
[22] White S R, 1992 *Phys. Rev. Lett.* **69** 2863
White S R, 1993 *Phys. Rev.* B **48** 10345
[23] Misguich G and Lhuillier C, 2004 *Frustrated Spin Systems* ed H T Diep (Singapore: World Scientific)
[24] Sindzingre A, 2004 *Phys. Rev.* B **69** 094418
[25] Parola A, Sorella S and Zhong Q F, 1993 *Phys. Rev. Lett.* **71** 4393
[26] Sandvik A, 1999 *Phys. Rev. Lett.* **83** 3069
[27] Wang X, Zhu N and Chen C, 2002 *Phys. Rev.* B **66** 172405
[28] Affleck I and Qin S, 1999 *J. Phys. A: Math. Gen.* **32** 7815
[29] Villain J, Bidaux R, Carton J-P and Conte R, 1980 *J. Physique* **41** 1263
[30] Azzouz M, Chen L and Moukouri S, 1994 *Phys. Rev.* B **50** 6233

J. Stat. Mech. (2006) P05007